Mon. Not. R. Astron. Soc. **386,** 1404–1410 (2008) doi:10.1111/j.1365-2966.2008.13044.x

ATCA observations of the very young Planetary Nebula SAO 244567

G. Umana,[1⋆] C. Trigilio,[1] L. Cerrigone,[2]† C. S. Buemi[1] and P. Leto[3]

[1]*INAF-Osservatorio Astrofisico di Catania, Via S.Sofia 78, Catania, Italy*
[2]*Universitá di Catania, Dipartimento di Fisica e Astronomia, Via S. Sofia 78, Catania, Italy*
[3]*INAF-IRA, Noto, C.P. 161, Noto(SR), Italy*

Accepted 2008 January 29. Received 2008 January 28; in original form 2007 September 18

ABSTRACT

The radio emission from the youngest known Planetary Nebula, SAO 244567, has been mapped at 1384, 2368, 4800, 8640, 16832 and 18752 MHz by using the Australian Telescope Compact Array (ATCA). These observations constitute the first detailed radio study of this very interesting object, as they allow us to obtain the overall radio morphology of the source and to compute, for the first time, the radio spectrum up to the millimetre range. The radio emission is consistent with free–free from a wind-like shell, which is also the region where most of the [O III] emission comes from as revealed by *Hubble Space Telescope* (*HST*) images. However, two other possible models, a uniform sphere and a uniform thin shell, can also reproduce the radio-observed quantities. Physical parameters of the radio nebula and of the central star were derived, for all the three proposed scenarios, all consistent with SAO 244567 being a very young Planetary Nebula still embedded in the dusty remnant of the asymptotic giant branch phase. The optically thin radio flux density appears to decrease when compared to data from the literature. The apparent variability of the radio emission, probably related to the evolution of the central object, needs further investigation.

Key words: stars: AGB and post-AGB – planetary nebulae: general – radio continuum: stars.

1 INTRODUCTION

The fate of a star with a main-sequence mass in the range from 1 to 8 solar mass is well established: it goes through the asymptotic giant branch (AGB) phase, then into the Planetary Nebula (PN) phase and eventually it will finish its evolution as a White Dwarf. However, the details of these evolutionary phases, such as the formation and the early evolution of PNe, are far from being completely understood. It is not clear, for example, which kind of mechanism changes the more or less regular and symmetric circumstellar envelopes (CSEs) around PNe progenitors (AGB stars) into the quite complex morphologies observed in young and more evolved PNe.

New clues on the process of PNe formation can be provided by the analysis of the physical characteristics of objects in the short phase between the end of the AGB and the onset of the ionization in the nebula. For this purpose, many authors have tried to identify very young Planetary Nebulae (YPNe) or proto-Planetary Nebulae (PPNe), but this is quite difficult as this evolutionary phase is very rapid and because the central object is often heavily obscured by the thick CSE formed during the AGB phase.

Among post-AGB objects, SAO 244567 appears to be unique, as it is evolving so rapidly that strong spectral and total luminosity changes were followed in a human life time-scale. Parthasarathy & Pottash (1989) classified SAO 244567 as a post-AGB star on the basis of its high galactic latitude and because its far-infrared (*IRAS*) colours are similar to those of known PNe. Very soon, it was realized that, in a few decades, its optical and ultraviolet spectra have developed characteristics typical of the presence of a nebula making SAO 244567 one of the youngest PN ever discovered (Parthasarathy et al. 1993).

In particular, its optical spectrum has evolved quite rapidly: reported by Henize (1976) with only *Hα* in emission, more recently, it has shown strong forbidden nebular emission lines, which are consistent with a YPN (Parthasarathy et al. 1995). These results confirm that SAO 244567 has turned into a PN within the last 20 yr and makes the source a perfect target for studying the early structure and evolution of PNe.

SAO 244567 was observed in 1996 with the Wide Field Planetary Camera 2 (WFPC2) (Bobrowsky et al. 1998). These observations showed that most of the nebular emission originates from a ring/ellipse, whose major axis extends for ∼1.6 arcsec, and the presence of low-density-collimated outflows. The authors interpreted the ring structure as the remnant of the mass-loss during the AGB phase, while the low-density bipolar structures result from the fast-wind experienced by the star during the post-AGB phase. The existence of a companion star, detected at 0.4 arcsec from the central star, indicates that the ring/ellipse is probably a circumbinary envelope and that, at least in this object, binarity may play an important role in the shaping. These images are some of the best examples

⋆E-mail: Grazia.Umana@oact.inaf.it
†SAO predoc fellow, Harvard-Smithsonian Centre for Astrophysics, Cambridge, MA 02138, USA.

where nebular structures, that appear to collimate fast outflows, are evident.

As typical for very YPN, SAO 244567 shows a strong infrared excess and it is associated with the *IRAS* source IRAS 17119−5926. Measured non-corrected *IRAS* fluxes are 0.65, 15.50, 8.20 and 3.52 Jy at 12, 25, 60 and 100 μm, respectively.

In spite of the numerous optical studies of this interesting object, very little is still known of its radio properties. Parthasarathy et al. (1993) briefly reported on Australia Telescope Compact Array (ATCA) 6 and 3 cm observations obtained in 1991. The measured flux densities, obtained by fitting to the visibilities, were 63.3 ± 1.8 and 51 ± 12 mJy at 6 and 3 cm, respectively.

In this paper, we present new ATCA observations of SAO 2444567 aimed to determine the radio properties of the nebula associated with this very YPN.

2 OBSERVATIONS

We carried out radio observations of SAO 244567 in 2000 March and 2002 August. In both epochs, the target was observed with the ATCA at Narrabri. The ATCA consists of six 22-m antennas, five of which lie along a 3 km railway track, oriented east–west, and the other antenna lies on a fixed station at 3 km away, thus providing a 6 km maximum baseline length.

As each ATCA antenna is equipped with dual-frequency systems, it is possible to observe simultaneously at two different frequency bands.

2.1 The 2000 data

In the first epoch, 2000 March, the observations were simultaneously performed at 6 (4800 MHz) and 3 cm (8640 MHz), with a 128 MHz bandwidth divided in 32 spectral channels, with an integration time of 30 s. The observations were carried out in the 6D configuration, which, with a full synthesis, usually provides a typical beam size ($\theta_{\rm syn}$) of about 2 arcsec at 6 cm.

The flux density scale was fixed by daily observations of the primary flux calibrator 1934−638, whose assumed flux densities are 5.83 and 2.84 Jy at 4800 and 8640 MHz, respectively. In order to achieve a good phase calibration, the phase calibrator 1718−649, which is 5.°5 away from SAO 244567, was observed interleaved with the source scans.

At this epoch, the source was observed in the context of a survey program aimed to detect radio emission from a sample of post-AGB stars. Therefore, for a good compromise between UV coverage and total integration time, the observations were performed in a snapshot mode, which consists of short *on-source* runs carried out at different hour angles. A typical observation of our target consisted of 7/8 cuts, each of 15 min long. In the case of SAO 244567, we observed the source with 14 cuts, for a total of 3.5 h. The observations were, however, obtained in different days starting from March 19 to 22.

Due to serious hardware problems at one of the antennas, the observations suffered from a degradation of the available angular resolution, resulting in a beam of 7.6 × 2.7 arcsec^2 at 6 cm much worse than the angular resolution achievable with the 6D configuration.

2.2 The 2002 data

We re-observed the source this time with a proper full track for better UV coverage. The observations were carried out on 2002 August 24 and 29. On both dates, the array was in 6C configuration. On August 24, we observed simultaneously at 16832 and 18752 MHz, with a 128 MHz bandwidth divided into 32 spectral channels, using an integration time of 30 s. At that time, only three antennas were equipped with mm backends. High-frequency observations are strongly affected by atmospheric phase fluctuations. To minimize this effect, we quickly switched between target and phase calibrator, with typical duty cycle of 6 min (4 min on target and 2 min on phase calibrator) for a total *on-source* time of 7 h. Reference pointing on our phase calibrator (1718−649) was also performed once per hour. The flux density scale was fixed by several observations of 1924−638, and the flux density of 1718−649 was bootstrapped using only those scans of the primary calibrator performed at the same elevation as 1718−649.

On August 29, the observations were carried out at 4800/8640 and at 1384/2368 MHz. The observations were performed following the same procedure as on August 24, using 1718−649 as phase calibrator, with a typical *on-source* scan of 15 min. However, only 30 per cent of the total *on-source* time of 10 h was spent observing at the lowest frequencies. The flux density scale was fixed relative to that of 1934−638 whose flux density is taken to be 14.94, 11.59, 5.83 and 2.84 Jy at 1384, 2368, 4800 and 8640 MHz.

3 RESULTS

The data from both epochs were reduced with the MIRIAD package, following the standard reduction steps as recommended in the MIRIAD User's Guide. Visibilities were weighted by applying robust weighting (robust parameter = 0.5). This method allows one to obtain the same sensitivity as with natural weighting but with a much better beam shape. Finally, the resulting maps were cleaned down to a few times the theoretical noise, estimated to be of the order of 0.1–0.2 mJy.

The map with the best combination of resolution and sensitivity is that obtained at 8640 MHz in 2002. The radio map (Fig. 1) reveals a slightly extended structure, whose overall size (∼1.7 arcsec) compares quite well with that observed in Hα (Bobrowsky et al. 1998). However, the limited ATCA angular resolution prevented us from discerning any fine detail of the radio structure.

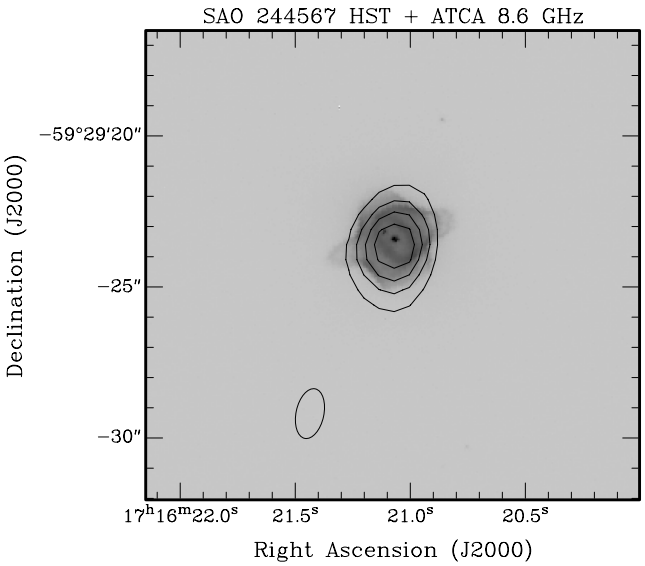

Figure 1. The radio map of SAO 244567 obtained with the ATCA at 8.4 GHz (contour levels) superimposed on the *HST* image in *Hα* (Bobrowsky et al. 1998). The synthetic beam is shown in the lower left corner.

Table 1. Summary of results: flux densities were determined by fitting of visibility curves.

Frequency (MHz)	Flux (mJy)	rms (mJy)	Phase cal flux (mJy)
Epoch 2000			
4800	57.6 ± 1.7	0.3	4500 ± 50
8640	52.0 ± 1.6	0.4	3400 ± 50
Epoch 2002			
1384	36.6 ± 1.1	0.2	
2368	46.9 ± 1.8	1.2	
4800	48.8 ± 1.5	0.2	5234 ± 20
8640	46.6 ± 1.4	0.2	4271 ± 20
16832	43.8 ± 2.0	0.3	
18752	42.8 ± 2.0	0.3	

The total flux density and the angular dimension can be usually estimated directly from the image, by a 2D Gaussian fit of the radio source. However, because an interferometer spatially filters out structures larger than the resolution corresponding to the minimum antenna spacing, the evaluation of flux density by a Gaussian fit becomes less precise for partially resolved sources. This effect will be more evident at higher frequencies. In this case, it is advisable to derive flux densities directly from the UV data, by fitting the visibilities at zero baseline. When the sources are angularly small, different methods to derive the flux density, i.e. from the map or from the fit to the visibility data, provide consistent flux density values to within a few per cent. In our case, differences between total fluxes measured in these two ways are of the order of 0.1 per cent up to 4800 MHz, but become more important at 18750 MHz where they increase up to ∼17 per cent. For this reason, in the following analysis we will consider the flux density derived from the visibility fits only. The results are summarized in Table 1, where the observing frequency, the measured flux density, with its associated σ and the rms of the visibility fit, are reported. An error in the flux calibration can result in a systematic error in flux density of the observed source. Therefore, the σ associated with the flux density estimation is derived from

$$\sigma = \sqrt{(\mathrm{rms})^2 + (\sigma_{\mathrm{cal}} S)^2}$$

where rms is the error associated with the fit, σ_{cal} is the error associated with the absolute flux density scale, which is accurate to within a few (3–5) per cents and S is the derived flux density.

In order to compare results from different epochs, for frequencies with multi-epoch data, we also report, in the last column of Table 1, the flux density of the phase calibrator (1718−649).

We note that the flux density at 4800 and 8640 MHz appears to decrease from 1991 (Parthasarathy et al. 1993) to 2002 (this paper). This decrement appears to be real and not related to a variation in the absolute flux scale as the flux density of the phase calibrator changes between the last two epochs but with a different trend, and it is actually increasing maintaining the same spectral index. In the following analysis, only the multifrequency epoch two data sets will be used.

4 THE NEBULA

4.1 The radio morphology

Some information on source morphology can be derived from the analysis of the visibility data, i.e. the fringe amplitude as a function of the interferometer spacing. Since the ATCA is a linear interferometer, each of the 15-min on-source scans (cuts) will give a maximum resolution in one direction and the corresponding visibility will be a function of the source morphology in that direction. Different visibilities corresponding to different cuts look quite similar and this indicates that the overall morphology of the radio source is symmetric with respect to a central point. The small elongation in the NW–SE direction reflects the UV coverage and therefore the synthetic beam with which the visibility data are convolved (see the lower left corner in Fig. 1) and it is not intrinsic to the source.

Table 2. Parameters of different models for the radio nebula around SAO 244567.

Parameter	Value
Model 1 (wind shell)	
Density	$n(R_{\mathrm{int}}) = 2.5 \times 10^4\ \mathrm{cm}^{-3}$, $n \propto R^{-2}$
Shell internal radius R_{int}	0.75 arcsec
Shell external radius R_{ext}	1.5 arcsec
Shell temperature	9600 K
Model 2 (shallow shell)	
Density	$n = 1.45 \times 10^4\ \mathrm{cm}^{-3}$
Shell internal radius	0.65 arcsec
Shell external radius	1.3 arcsec
Shell temperature	10000 K
Model 3 (sphere)	
Density	$n = 1.23 \times 10^4\ \mathrm{cm}^{-3}$
Sphere size	1.4 arcsec
Sphere temperature	10 000 K

We have modelled the visibilities of the entire observing run, averaged over 15 min, assuming three different symmetric morphologies for the radio source, i.e. Model 1: a shallow shell, 0.75 arcsec thick, with an external radius of 1.5 arcsec a density decreasing with distance from the central star ($n \propto \frac{1}{r^2}$); Model 2: a constant density shallow shell, 0.65 arcsec thick and an external radius of 1.3 arcsec and Model 3: a constant density sphere, with a radius of 1.4 arcsec.

The best-fitting parameters of the three models are summarized in Table 2 and results, relative to the visibilities observed at 8640 MHz, are shown in Fig. 2. In the first panel, the expected visibility from a stellar wind, extending to infinity, is shown (dotted line) for comparison. From this analysis, we may conclude that the source morphology is consistent with both a shallow shell (with constant or with $\propto \frac{1}{r^2}$ density) and with a constant density sphere.

4.2 The physical properties

Information on several parameters of a radio source can be derived by analysing its radio spectrum, in particular when the transition region between the optically thick and optically thin regimes can be pointed out. The analysis of the visibility data indicates a symmetric morphology, consistent with both a constant density sphere and a wind or constant density shell. Very little studies on modelling of free–free radio spectrum of PNe have been conducted, mostly because of the very few multifrequency spectra available in the literature. Among them, Aaquist & Kwok (1991), by analysing a sample of compact (young) PNe, noted a trend of an increasing value of the spectral index α (flux $\propto \nu^{\alpha}$), evaluated in the optically thick part of the spectrum, as the turnover frequency (ν_{c}) decreases. This was interpreted as evidence, in the very early stages of nebula

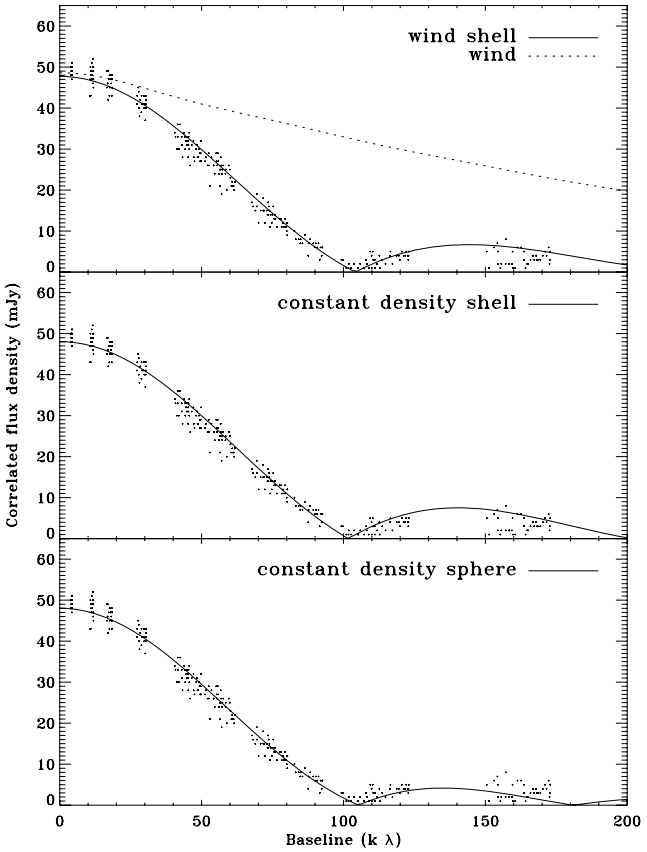

Figure 2. Comparison between different modelling of the radio source. Both a shallow shell (with density $\propto \frac{1}{r^2}$ or constant) and a constant density sphere are consistent with the observed visibilities. A stellar wind extending to infinity is shown as an example.

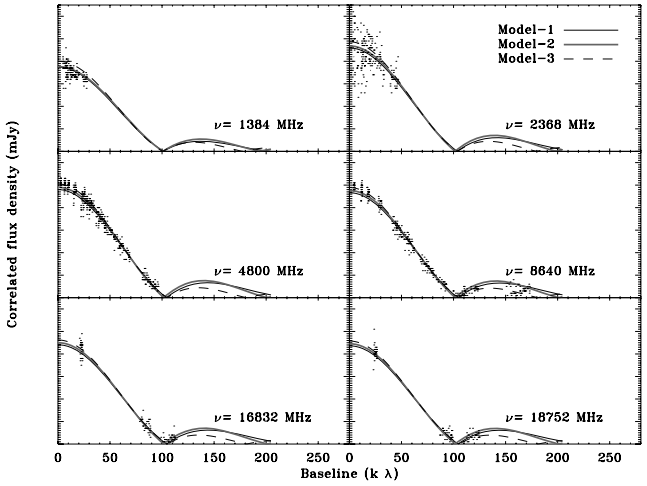

Figure 3. The modelling of visibilities at various frequencies. Different lines correspond to different assumed models for the radio source.

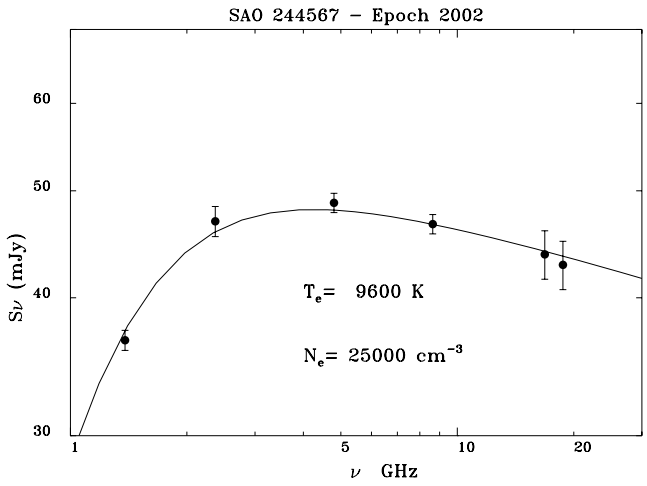

Figure 4. The observed flux densities superimposed to the radio spectrum of SAO 244567 obtained assuming a shell, 0.75 arcsec thick, with decreasing density ($\propto r^{-2}$), with $T = 9600$ K and $n = 2.5 \times 10^4$ cm^{-3} at the inner radius.

evolution, for most of the free–free emission coming from the AGB progenitor's wind, with typical $\alpha = 0.6$. Taylor, Pottasch & Zhang (1987) modelled the radio continuum of 18 compact PNe with a shell model, with a radially dependent density. The observed radio spectra are well represented by a wind shell, supporting the idea that free–free originates from a region formed with a constant stellar mass loss during the preceding red giant phase.

These previous results, together with the fact that SAO 244567 is a very YPN, may lead us to assume a wind-shell morphology as the most probable morphology for SAO 244567. However, all the proposed models reproduce the observed visibilities at all the observed frequencies (Fig. 3). While Models 1 and 2 are indistinguishable, an appreciable difference is evident for Model 3 but only at the highest baselines, which are, however, not well sampled by the present ATCA observations. Also the radio spectra, derived for each model, are all very similar, presenting a turnover frequency, i.e. the frequency at which the nebula becomes transparent, between 2368 and 4800 MHz. As an example, the modelled radio spectrum, obtained for Model 1, superimposed to the observed data, is shown in Fig. 4. Since from the measured radio quantities it is not possible to distinguish among different models, in the following we will derive several physical parameters by considering different physical conditions in the radio nebula, corresponding to the different models.

An estimate of the total ionized mass contained in nebula can be obtained by integrating the density of ionized particles over the radio emitting region, assuming for each proposed model the proper geometry. In the hypothesis of a pure hydrogen nebula at 5.6 kpc (Parthasarathy et al. 1993), we derive a total ionized mass of $\sim$0.065 M$_\odot$, for Model 1, $\sim$0.057 M$_\odot$ for Model 2 and $\sim$0.07 M$_\odot$ for Model 3. These values depend on the value of the volume filling factor of the nebula, which has been assumed to be 1.

A similar value was derived by Parthasarathy et al. (1993), who, however, did not specify the method used in deriving the nebular mass. Bobrowsky (1994) obtained a value of 0.2 M$_\odot$ from the $H\beta$ flux, by applying a relation that is valid for a spherical nebula containing ionized material, consisting of 10 per cent of He, with a uniform electron density. The radio model that better reproduces the nebular model used to derive the formula as in Bobrowsky (1994) is Model 3 (sphere, with a uniform density). Adopting the formula for the case of a pure hydrogen nebula and assuming the nebular temperature and density as from Model 3, we derive from the $H\beta$ flux (Bobrowsky 1994) a total ionized mass of $\sim$0.1 M$_\odot$, that, within errors, is closer and thus more consistent with the values obtained from the radio data.

Since the recombination lines and free–free radio continuum originate from the same ionized region, the radio optically thin flux density can be related to the flux measured in these lines (Pottasch 1984). The comparison between the observed line flux to the value derived from the radio flux density provides a way to evaluate the extinction towards the nebula. This is, however, a measurement of the combination of both external and intrinsic extinction along the line of sight. Parthasarathy et al. (1993), by applying this method to the radio and $H\beta$ fluxes, derive a $E(B-V) = 0.14$ to the nebula. However, because of the observed variability of radio flux density of SAO 244567 and of the lack of recent $H\beta$ flux determinations, from the measurements of the present paper, it is not possible to derive any information on the internal plus external extinction.

We can use the observed radio optically thin flux density plus the angular size to derive the mean emission measure as follows (Terzian & Dickey 1973):

$$\langle \mathrm{EM} \rangle = \frac{\int_\Omega \mathrm{EM} d\Omega}{\Omega} = \frac{5.3\,10^5 F_{8.4}}{\theta^2} = 1.1 \times 10^7\ \mathrm{cm}^{-6}\ \mathrm{pc},$$

where $F_{8.4}$ is the measured radio flux density, in mJy, at 8.4 GHz, and θ, in arcsec, the angular dimension of the radio emitting region as derived from the specific model. The previous value has been determined in the case of Model 1. The EM value changes to 1.5×10^7 and $1.2 \times 10^7\ \mathrm{cm}^{-6}$ pc for Models 2 and 3, respectively.

YPNe should have emission measures of the order of 10^6–$10^8\ \mathrm{cm}^{-6}$ pc (Terzian & Dickey 1973; Kwok, Purton & Keenan 1981).

In the hypothesis of a constant density nebula, we can also derive the excitation parameter (U_{exc}) required to account for the measured radio flux density:

$$U_{\mathrm{exc}} = 13.3\left(\nu^{0.1} T^{0.35} D_{\mathrm{Kpc}}^2 F_\nu\right)^{\frac{1}{5}}\ \ \mathrm{pc\ cm}^{-2}, \quad (1)$$

where F_ν is the optically thin radio flux density, expressed in Jy, at the observing frequency ν (in GHz); T is the nebula temperature, expressed in 10^4 K, and D_{Kpc} is the source distance in Kpc.

As the PN associated with SAO 244567 is very young, we can assume that it is ionization bounded; in this case, the excitation parameter is directly related to the number of ionizing photons emitted by the central star.

$$L_{\mathrm{uv}} = 1.23 \times 10^{56} \beta U_{\mathrm{exc}}^3\ \ \mathrm{photons\ s}^{-1}, \quad (2)$$

where β is the hydrogen recombination coefficient summed over all levels above the ground level ($\sim 3 \times 10^{-13}\ \mathrm{cm}^3\ \mathrm{s}^{-1}$ for $T \sim 10^4$ K) (Spitzer 1978).

From equations (1) and (2), assuming a nebular temperature of $T \sim 9600$ K and a distance of 5.6 Kpc, from the radio flux density measured at 8.6 GHz, we derive a number of ionizing photons of $L_{\mathrm{uv}} \sim 1.53 \times 10^{47}$ (photons s^{-1}).

To test the dependence of the number of ionizing photons on the density model assumed for the radio source, we used the formula reported by Taylor et al. (1987) (their formula 10), which is valid for a thin, wind-like shell and, for a ratio between the inner radius to the external radius equal to 0.5, reproduces the situation of our Model 1. We derive a $L_{\mathrm{uv}} \sim 6.25 \times 10^{47}$ (photons s^{-1}), indicating that, in the case of a gradient in the electron density, the number of ionizing photons, derived by means of the excitation parameter, can be underestimated. We conclude that, in the hypothesis of a constant density source (i.e. Models 2 and 3) the derived L_{uv} indicates a central object whose Lyman continuum photon flux corresponds to a B0–B0.5 V star, while, if the radio nebula possesses a density gradient, the central object has a Lyman continuum photon flux corresponding to a O9.5-B0 V star (Panagia 1973). This translates to an effective temperature of $T_{\mathrm{eff}} \sim (2.8 \pm 0.2) \times 10^4$ K and $T_{\mathrm{eff}} \sim (3.2 \pm 0.1) \times 10^4$ K, respectively.

These values for the effective temperature of the central star are somewhat lower than the value of $T_{\mathrm{eff}} \sim 3.7 \times 10^4$ K estimated by Parthasarathy et al. (1993) from the analysis of the UV spectra and corresponding to a O8V star. This may indicate the presence of a significant quantity of dust well mixed with the gas in the inner regions of the nebula. Dust, in fact, competes with the gas for the absorption of the ionizing photons and for a given number of ionizing photons emitted by the central star, it will also reduce the observed radio flux density.

5 THE DUSTY ENVELOPE

One of the most important results from PNe studies based on *IRAS* data was the realization that, on average, in YPNe about 40 per cent of the emergent flux is emitted in the far-infrared (Zhang & Kwok 1991). This is due to the presence of an extended dusty envelope, around YPNe, which is the remnant of the precursor's wind not yet dispersed. In YPNe, the spectrum emitted by the dust, between 10 and 100 μ m, is usually well described by a single temperature blackbody curve (Zhang & Kwok 1990; Stasinska & Szcerba 1999). We therefore derive a dust temperature of $T_{\mathrm{dust}} = 137 \pm 2$ by using a least-squared fitting procedure to the *IRAS* measurements. This procedure provides, as a byproduct, the total far-infrared flux (F_{IR}), obtained by integrating, over the *IRAS* band (25 to 100 μm), the Planck curve that fits the *IRAS* data.

It is therefore possible to define the far-infrared excess (IRE) as the ratio of the observed total far-infrared flux (F_{IR}) over the expected total infrared flux. Under the hypothesis that the far-infrared flux is due to thermal emission from dusty grains heated by Lyα photons, this ratio is unity. However, in young PNe heating by direct starlight is important and IRE can be much higher than unity. Pottasch (1984) has derived a formula to express the expected total infrared flux in terms of optically thin radio flux density:

$$\mathrm{IRE} = 1.07 \frac{F_{\mathrm{IR}}}{F_{8.6\,\mathrm{GHz}}} = 2.8,$$

where F_{IR} is expressed in $10^{-14}\ \mathrm{W\ m}^{-2}$, $F_{8.6\,\mathrm{GHz}}$ in mJy and the high-density approximation has been adopted. This value is consistent with the hypothesis that SAO 244567 is a very YPN where the dust plays an important role.

To quantify the total mass of the dust, we will use the optically thin expression (Hildebrand 1983):

$$M_{\mathrm{dust}} = \frac{F_{60\,\mu\mathrm{m}} D^2}{\chi B\nu(T_{\mathrm{dust}})},$$

where $F_{60\,\mu\mathrm{m}}$ is the flux density measured at 60 μ m, D is the distance to the source (Kpc), $B\nu(T_{\mathrm{dust}})$ is the value of the BB function of T_{dust}, evaluated at 60 μm and χ is the mean absorption coefficient for the grains ($\mathrm{cm}^2\ \mathrm{g}^{-1}$). This formula provides only an estimation of the total dust mass at a single temperature and a single size for the grains is assumed. Moreover, while this dust mass determination is independent of the distribution of the grains, it strongly depends on the chemical composition of the grains.

There are still problems in understanding the chemical composition of the dust component in PNe. Usually, in carbon-rich PN, dust is mainly composed of carbon-based grains, while in O-rich PN, dust is mainly composed of different forms of silicates. As for SAO 244567, we do not have any information on its chemical composition, we compute the dust mass for two different values of χ, namely 53.45 $\mathrm{cm}^2\ \mathrm{g}^{-1}$, which corresponds to circumstellar silicates

and 145.32 cm^2 g^{-1}, which corresponds to graphite (Stasinska & Szcerba 1999). This results in a total dust mass of $2 \times 10^{-4}\,M_\odot$, in case of silicates, and $7.5 \times 10^{-5}\,M_\odot$, in case of graphite. If we assume that dust and gas occupy the same volume, we may derive a dust-to-gas ratio of 3×10^{-3} and 1.15×10^{-3} for silicates and graphite, respectively. Considering the other two models for the radio nebula, we obtain quite similar values, i.e. 3.5×10^{-3} and 1.3×10^{-3}, for Model 2 and 2.8×10^{-3} and 1.07×10^{-3} for Model 3. These values are in the range for $M_{\rm dust}$ and $M_{\rm gas}$ derived for a large sample of PNe (Stasinska & Szcerba 1999).

6 THE VARIABILITY OF RADIO EMISSION

One of the most striking and unexpected characteristics of radio emission from SAO 244567 is its variability. In Fig. 5, we plot the flux density at 4800 MHz, as measured by Parthasarathy et al. (1993) and in this paper, indicating a linear decreasing trend of the optically thin flux density. The dashed line is the weighted fit to the 4800 MHz data points, which results in a flux density decrement of ∼1.3 mJy yr^{-1}. Assuming that the radio emission from the source will keep this trend, a flux density of ∼43 mJy in 2008 is predicted. In the same figure, we also include the 2000 and 2002 data at 8640 MHz, without considering the quite noisy datum from Parthasarathy et al. (1993). In a YPN, we expect the radio emission to change quite drastically due to the variations of the physical conditions of the central star and of the nebula. During the early development of the radio nebula, the radio flux density is expected to increase as a consequence of (i) the increasing temperature of the central star and (ii) the increase of the total ionized mass, due to the combined effect of (i) and of the nebula's expansion. A decrease of the optically thin radio flux density may be observed only in the later phases of nebula's evolution, after that the full ionization of the nebular mass has occurred (density-bounded nebula), but this should not be the case of SAO 244567 as it appears to be very young. However, we may assume that SAO 244567 is already in the density-bounded phase and verify under which circumstances it is possible to reproduce the observed decrease in the radio flux density. In the hypothesis that, between 2000 March and 2002 August (ΔT), the ionized mass remains the same, any effects due to the evolution of the central object can be neglected, and the nebula is expanding uniformly, we have

$$M_{\rm Tot} \propto n_{2000} R_{2000}^3 = n_{2002} R_{2002}^3. \quad (3)$$

Starting from the results for epoch 2002, from equation (3) we obtain constraints for epoch 2000. To reproduce the flux density observed at 4800 and 8640 MHz in epoch 2000, we then used the model, as illustrated in Sections 4.1 and 4.2, obtaining a reasonable fit for $T_{\rm eff} = 9600$ K, as in the 2002 fit, with an internal radius of 0.71 arcsec, an external radius of 1.4 arcsec and a density, at the base of the shell, of $n_{2000} = 2.9 \times 10^4$ cm^{-3}. To obtain such an expansion, we need the nebula to expand in a time ΔT with an average velocity of ∼850 km s^{-1}. Similar values for the expansion velocity are obtained when the other models were considered. We should stress here that a variation of radius of the order of a few 0.1 arcsec would not be detectable with present instrumentation (ATCA).

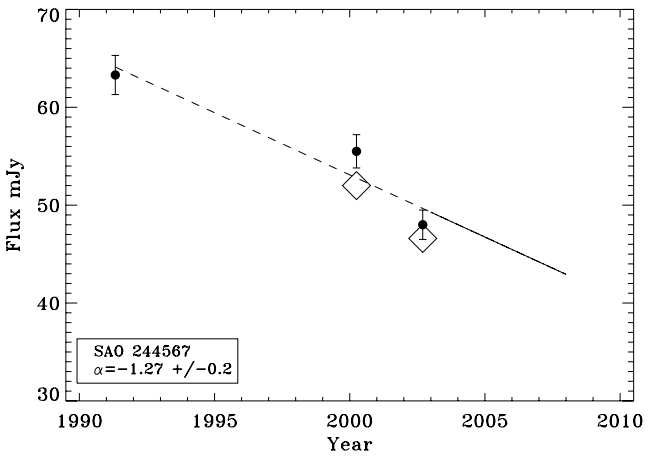

Figure 5. The behaviour of flux density of SAO 244567 as measured at 4800 MHz, filled dots. Data are from Parthasarathy et al. (1993) and this paper. A weighted fit to the data is also shown, which predicts a radio flux density at this frequency of 43 mJy at the beginning of 2008. Measures at 8640 MHz are also plotted as diamonds.

High expansion velocities have been observed in the ultraviolet lines of some PPNe and YPNe (Gauba et al. 2001) and are usually related to fast-wind events occurring during the post-AGB phase. For SAO 244567, Parthasarathy et al. (1995) reported, in 1988, an ultraviolet spectrum characterized by strong P-Cyg profiles, indicating the presence of a strong wind with expansion velocities of the order of ∼3000 km s^{-1}. These spectral structures were observed until 1993, and by 1994 they had almost vanished, indicating the end of a rapid mass-loss event. At the same time, Parthasarathy et al. (1993) derived, from high-resolution [O III] profiles, an expansion velocity of the order of ∼8 km s^{-1}, consistent with the fact that the ionized shell, from which most of the [O III] emission comes from, is the remnant of mass-loss during the previous AGB phase. Both results are consistent if we assume that UV lines are produced in the low-density polar region, where an episodic rapid mass-loss event can occur, while the bulk of the ionized material, and also the radio emission, is localized in the main ring/shell, as indicated by the *Hubble Space Telescope* (*HST*) images, which is expanding with typical velocity as expected for a AGB wind. Therefore, we may conclude that an expansion of the main shell cannot explain the observed decrement in the radio flux density because the required expansion velocity is too high.

High-velocity mass-loss events may, however, contribute to the total ionization of the nebula. This is what is claimed by Sanchez Contreras et al. (2004) to explain the decrease in millimetric, free–free optically thin flux density observed in the PPNe CRL 618. According to these authors, in this source there is a substantial contribution of shocks, originating from interactions between the fast post-AGB wind with the CSE environment, to the total ionization. As the fast-wind stops, the ionization relies only on the central star radiation field and the optically thin radio emission is, therefore, decreasing. However, this explanation requires episodic high-velocity mass-loss events to justify the flux density increase reported by the same authors 2 yr later (Sanchez Contreras et al. 2004b). A decrease in the optically thin flux density has also been noted in NGC 7027 (Zijlstra, Perley & van Hoof 2007) and it is interpreted as related to the evolution of the central object. NGC 7027 is located just at the tip of the WD cooling track, where its luminosity starts to decrease while its temperature is still increasing. This leads to a decreasing number of ionizing photons. Since the optically thin free–free emission is directly relating to the ionizing flux from the central star, this would imply a decreasing optically thin radio flux density.

SAO 244567 has shown many spectral changes in the last 20 yr. Most notably, the changes in the UV flux level, which suffered a factor of 2.83 decrement in 7 yr, while the central star was gradually becoming hotter (Parthasarathy et al. 1995), implying a total drop of the central star luminosity. This places the central star of

SAO 244567 in the same position on the HR diagram as NGC 7027 (Zijlstra et al. 2007), just on the top of the cooling WD track. However, as already pointed out by Parthasarathy et al. (1995), Bobrowsky et al. (1998), such a very fast evolution is very difficult to explain in the framework of actual post-AGB evolutionary models, that for a core mass object of $\sim 0.056\,M_{\odot}$ (Parthasarathy et al. 1993), predicts a much slower evolution (Schonberner et al. 2005).

7 SUMMARY

We have presented ATCA multi-epoch, multifrequency observations of the YPNe SAO 244567, aimed to derive its radio characteristics to complete the picture of this quite intriguing object. The best radio map, for sensitivity and resolution, has been obtained at 8640 MHz (3.6 cm), which reveals a slightly extended radio structure. ATCA does not resolve the fine details of the nebula as shown by *HST* observations. However, some morphological information has been derived by fitting a model to the observed visibility data, which are consistent with a wind-like shell whose external radius is in agreement with that of the main structure observed by *HST*.

Actual models for the early evolution of PNs radio spectra consider a wind-type density distribution, as a consequence of the ionization of the previous AGB wind, supporting a wind-shell morphology for the radio source. However, on the basis of the observed radio quantities other two models cannot be ruled out: a shallow-shell and a uniform sphere, both with constant density and dimensions still comparable to those observed by *HST*. From the present observations, we derived several physical parameters for the radio nebula, taking into account the different proposed morphologies. The mean emission measure and the infrared excess are consistent with a very YPN, still embedded in its dusty envelope, a remnant of the earlier AGB phase. By comparison between the total ionized gas mass, as derived from the radio, and the total dust mass, as derived from the *IRAS* data, a dust-to-gas ratio has been derived, by considering two different types of chemistry for the dusty envelope.

When compared with previous observations, the radio flux density appears to vary. In particular, the decrement of the 6 cm flux density (from 1991 to 2002) does not agree with an expansion of the main shell but appears to be related to the characteristics of the stellar object, whose fast evolution is difficult to explain in the framework of the recent models of post-AGB evolution. Further multifrequency monitoring and mapping with the ATCA fully equipped with millimetre receivers are necessary to confirm variation with a longer time baseline. Up to now, a variation (decrement) of the optically thin radio emission has been observed only in two other objects: the proto-PN CRL 618 and the PN NGC 7027. In both cases, the observed variations have been interpreted in terms of the evolution of the central object. The paucity of objects where such variations have been followed makes further radio observations of SAO 244567 very important, as typical time-scales of such variations can be used to test current evolutionary models.

ACKNOWLEDGMENTS

The ATCA is part of the Australian Telescope which is funded by the Commonwealth of Australia for operation as a National Facility managed by CSIRO. The authors wish to thank the anonymous referee for her/his helpful review.

REFERENCES

Aaquist O. B., Kwok S., 1991, ApJ, 378, 59
Bobrowsky M., 1994, ApJ, 426, L47
Bobrowsky M., Sahu K. C., Parthasarathy M., García-Lario P., 1998, Nat, 392, 469
Gauba G., Parthasarathy M., Nakada Y., Fujii T., 2001, A&A, 373, 572
Henize K. G., 1976, ApJS, 30, 491
Hildebrand R. H., 1983, QJRAS, 24, 267
Kwok S., Purton C. R., Keenan D. W., 1981, ApJ, 250, 232
Panagia N., 1973, AJ, 78, 929
Parthasarathy M., Pottasch S. R., 1989, A&A, 225, 521
Parthasarathy M., Garcia-Lario P., Pottasch S. R., Manchado A., Clavel J., de Martino D., van de Steene G. C. M., Sahu K. C., 1993, A&A, 267, L19
Parthasarathy M. et al., 1995, A&A, 300, L25
Pottasch S. R., 1984, ASSL, 107, Planetary Nebulae – A Study of Late Stages of Stellar Evolution. D. Reidel Publishing Co, Dordrecht.
Sanchez Contreras C., Sahai R., 2004, ApJ, 602, 960
Sanchez Contreras C., Bujarrabal V., Castro-Carrizo A., Alcolea J., Sargent A., 2004, ApJ, 617, 1142
Schonberner D., Jacob R., Steffen M., Perinotto M., Corradi R. L. M., Acker A., 2005, A&A, 431, 963.
Spitzer L., 1978, Physical Processes in the Interstellar Medium. Wiley-Interscience, New York
Stasinska G., Szczerba R., 1999, A&A, 352, 297
Taylor A. R., Pottasch S. R., Zhang C. Y., 1987, A&A, 171, 178
Terzian Y., Dickey J., 1973, AJ, 78, 875
Zhang C. Y., Kwok S., 1990, A&A, 237, 479
Zhang C. Y., Kwok S., 1991, A&A, 250, 179
Zijlstra A., Perley R., van Hoof P., 2007, NRAO Newsletter, 111, 7

This paper has been typeset from a TEX/LATEX file prepared by the author.